# Cluster Angular Spreads in a MIMO Indoor Propagation Environment

Nicolai Czink, Ernst Bonek
Institut für Nachrichtentechnik und Hochfrequenztechnik
Technische Universität Wien, Austria
Email: {nicolai.czink,ernst.bonek}@tuwien.ac.at

Xuefeng Yin, Bernard Fleury
Department of Communication Technology
Aalborg University, Denmark
Email: {xuefeng,bfl}@kom.auc.dk

***Abstract*— An important parameter of MIMO channel models is the cluster root-mean-square (rms) directional spread. In this paper we determine this parameter in the angle-of-arrival/angle-of-departure (AoA/AoD) domain based on comprehensive indoor MIMO measurements at 5.2 GHz in a cluttered office environment. This is done in a four-step procedure: (i) the SAGE algorithm is used to extract propagation paths, (ii) clusters of estimated paths in the double-azimuth domain are defined, (iii) the estimated propagation paths are allocated to the clusters, (iv) the cluster spreads are estimated based solely on propagation paths within the clusters. We found that the spreads are different when seen from transmitter or receiver due to different propagation conditions resulting in AoD rms cluster spreads lying in the range from 2 to 9 degrees and AoA rms cluster spreads in the range from 2 to 7 degrees.**

## I. Introduction

The use of multiple antennas at both link ends (MIMO) in wireless communications promises high spectral efficiency and reliability. Accurate channel models are required for proper design of signal processing algorithms. An important feature of the MIMO propagation channel with respect to MIMO applications is the occurrence of multi-path components (MPCs) in clusters. The authors of [1] have shown that channel models disregarding clustering effects overestimate channel capacity. Several new models assume clustered propagation paths, where propagation paths within a cluster show a distinct "angular spread" [2], [3]. In this paper we use the measure of the "directional spread" as it is a more accurate description of the spread of the MPCs. Please refer to [4] for detailed discussion of the different meanings and implications.

In our understanding "clusters" are a group of MPCs showing similar AoA, AoD, and delay, though we disregard the delay domain in this paper.

Previous results on the angular spread of *clusters* were obtained mostly for single-input multiple-output (SIMO) channels in the AoA/delay-domain. Using SAGE for estimating channel parameters, the authors of [2] investigated the distribution of cluster position, the distribution of MPCs' position per cluster, and the number of clusters and distribution of the number of MPCs per cluster. They find a mean number of 7 clusters in their scenarios. Using a spatial filter on SAGE estimates, [5] investigated the cluster angular spread and observe mean cluster angular spreads of 8 - 30 degrees. (Note that these spreads are not rms values.) In [3], variances of the (assumed) Laplacian distribution of cluster angular spreads were found in the range from $21.5$ to $25.5$ degrees. The number of clusters and the average clusters rms angular spread were also investigated in [6]. The authors found an average number of only $2.3$ clusters but rms angular spreads of 27 degrees by using the CLEAN algorithm [6].

Based on a comprehensive indoor MIMO measurement campaign we investigate the cluster directional spread in the joint AoA/AoD-domain, as this is an important prerequisite for MIMO applications.

## II. Measurement

### A. Measurement set-up

For the measurements [7], we used the wideband vector channel sounder RUSK ATM [8] with a measurement bandwidth of 120 MHz at a center frequency of 5.2 GHz. At the transmitter (Tx) side, a sleeve antenna was mounted on a 2D positioning table where the position was controlled by the channel sounder by means of two stepping motors. The Tx antenna was moved to 20 possible x- and 10 possible y-positions on a rectangular grid with $\lambda/2$ spacing, forming a $10 \times 20$ virtual Tx uniform planar array *without* mutual coupling. The receiver (Rx) was equipped with a directional 8-element uniform linear array (ULA) with $0.4\lambda$ inter-element spacing and two additional dummy elements. The antenna elements were printed dipoles with a backplane with $120^\circ$ 3dB field-of-view; they were consecutively multiplexed to a single receiver chain.

For each Tx position the channel sounder measured 128 temporal snapshots of the frequency-dependent transfer function between the Tx monopole and all Rx antennas. Within the measurement bandwidth of 120 MHz, 193 equidistant samples of the frequency transfer function were taken. Altogether, this resulted in a ($128\times193\times8\times200$) 4-dimensional complex channel transfer matrix containing the samples of the transfer function for each temporal snapshot, frequency, Rx and Tx position. Since the measurement of the whole channel transfer matrix took about 10 minutes, we measured at night to ensure stationarity. In a post-processing step, all 128 temporal snapshots were averaged to increase the signal-to-noise ratio (SNR), furthermore the mutual coupling effects in the receiver array were cancelled using the method proposed in [9]. For

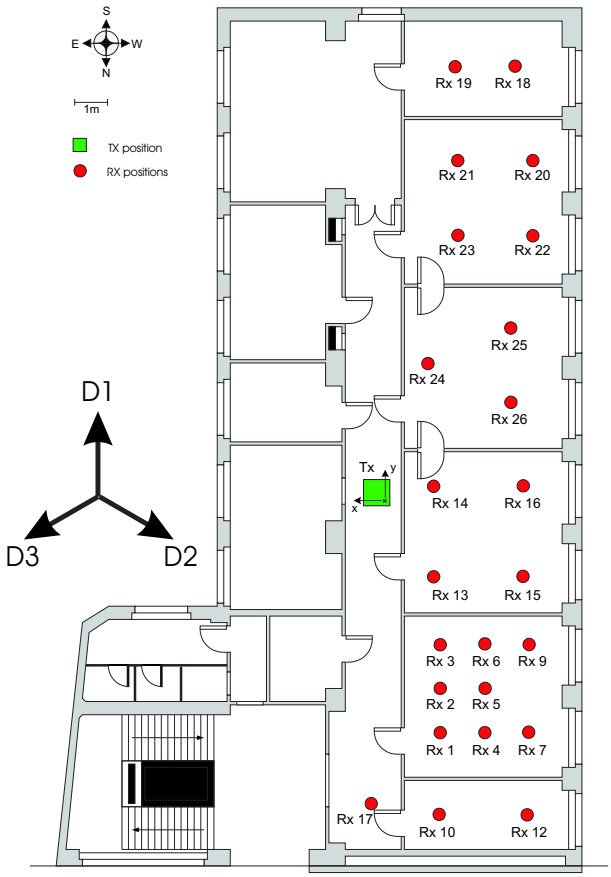


Fig. 1. Map of measured indoor scenarios

the following evaluations, we used only a sub-array of $6 \times 12$ Tx positions to mitigate large-scale fading effects.

### B. Environment

The measurements were carried out in the offices of the *Institut für Nachrichtentechnik und Hochfrequenztechnik, Technische Universität Wien*. In total, 24 Rx positions were measured: one in a hallway - with line-of-sight (LOS) to Tx, 23 of them in several office rooms connected to this hallway - with non-line-of-sight (NLOS) to Tx, always with the (virtual) Tx array positioned in the same place in the hallway. Some rooms were amply, others sparsely furnished with wooden and metal furniture, bookshelves, and plants. Figures 2 and 3 show photographs taken from the equipment positioned in the corridor, and an exemplary scenario in one of the office rooms, respectively. At each position, we rotated the Rx antenna to three different broadside directions D1, D2 and D3 (see Figure 1). These directions were angularly spaced by $120°$. Thereby, we get 72 different "scenarios", i.e. combinations of Rx positions and directions.

In this paper we consider multiple realisations of $8 \times 8$ MIMO channels and discard delay-dispersion. Spatial realisations were generated by always considering all Rx antennas and grouping 8 adjacent transmitter positions together [7, Ch. 4.3.3]. Doing this for all possible Tx positions yields a number of 30 spatial realisations. Additionally all 193 frequencies were

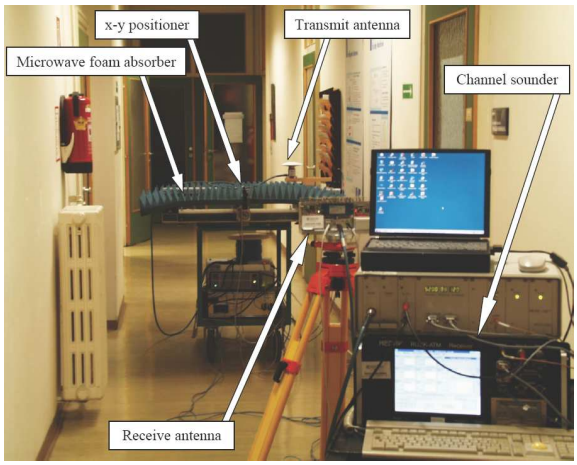


Fig. 2. Measurement equipment positioned in the corridor

Fig. 3. Exemplary scenario in one office room (position Rx7D2)

considered as realisations which yields a total number of 5790 channel realisations per scenario.

## III. Evaluation

The estimation of the cluster directional spread was done in four steps: MPC estimation using the SAGE algorithm, cluster identification, cluster path allocation and cluster spread estimation.

### A. SAGE estimation

For each scenario, out of all 5970 channel realisations we randomly selected a subset of $K = 150$ different channel realisations to keep the computational complexity tractable. The $8 \times 8$ MIMO channel matrices are denoted by $\mathbf{H}_k$, where $k = 1 \ldots K$ denotes the $k$th realisation.

Subsequently, we apply the SAGE algorithm [10] (implementation from [11]) individually to each of the channel realisations $\mathbf{H}_k$ to estimate the complex weights, AoAs, and AoDs of the propagation paths. We chose the maximum number of MPCs equal to 49 in order to extract as many paths as possible for $8 \times 8$ MIMO systems. The dynamic range was set to 30dB to be well within the SNR level of our measured channel realisations.

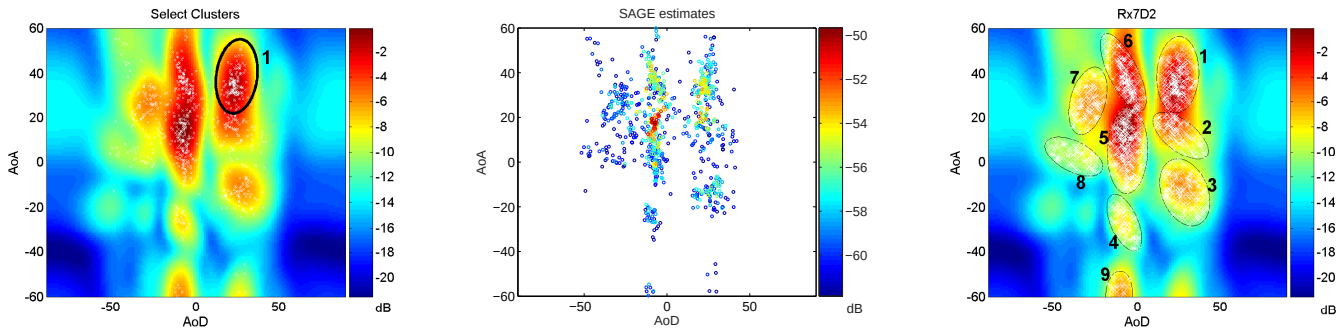


(a) (b) (c)

Fig. 4. Cluster identification and path allocation: (a) Azimuth power spectrum with SAGE estimates, (b) SAGE estimates solely, (c) identified clusters with allocated propagation paths within the clusters

### *B. Cluster identification*

Throughout literature (e.g. [2], [5]), clusters are identified visually, as clustering algorithms are either too time consuming or do not work properly [3], [6]. We also adopt this approach, but improve it by using the double-directional azimuth power spectrum (APS) jointly with SAGE estimates of the MPCs.

Once clusters have been identified, the directional distributions can be determined. One has to be careful with the estimation of the cluster directional spread. Evolving from the propagation model used, directional distributions are not correctly reproduced by high-resolution estimation algorithms that are based on the specular path model [12]. The direction estimates show a heavy-tailed distribution. We truncate this heavy tail by *limiting our clusters within ellipses* and thus circumvent this effect.

For visual cluster identification, we use the following method. Channel matrices are averaged by using the full spatial correlation matrix, $\mathbf{R_H}$, which is estimated by

$$\mathbf{R_H} = \frac{1}{K}\sum_{i=1}^{K} \mathrm{vec}(\mathbf{H}_k)\mathrm{vec}(\mathbf{H}_k)^H, \tag{1}$$

where $(\cdot)^H$ denotes hermitian transpose, and the $\mathrm{vec}(\cdot)$ operator stacks the columns of the matrix given as an argument into a vector. By this, we average over small-scale and frequency selective fading effects.

The double-directional azimuth power spectrum (APS) [13] is calculated using the Bartlett beamformer [14] by

$$P(\varphi_{\mathrm{Rx}}, \varphi_{\mathrm{Tx}}) = \tilde{\mathbf{a}}^H\, \mathbf{R_H}\, \tilde{\mathbf{a}}, \text{ with } \tilde{\mathbf{a}} = \mathbf{a}_{\mathrm{Tx}}(\varphi_{\mathrm{Tx}}) \otimes \mathbf{a}_{\mathrm{Rx}}(\varphi_{\mathrm{Rx}}), \tag{2}$$

where $\otimes$ denotes the Kronecker product, $\mathbf{a}_{\mathrm{Tx}}(\varphi_{\mathrm{Tx}})$ the normalised steering vector of the virtual Tx array, and $\mathbf{a}_{\mathrm{Rx}}(\varphi_{\mathrm{Rx}})$ the normalised response vector of the Rx array.

To find multipath clusters, we plot two figures: (i) the APS (2), jointly with the 1000 strongest SAGE estimation points, and (ii) these SAGE estimates only, but colour-coded, indicating their power. Then we identify clusters by following rules:

- "Clusters" are defined as a group of MPCs showing similar AoA and AoD.
- In the SAGE plot, clusters show dense SAGE estimates with similar powers, where the powers of the MPCs decrease from the cluster's centre to the outskirts.
- In the APS the cluster's power must also be decreasing from the centre to the outskirts.
- Clusters must not overlap.

Using these rules, one can visually fit ellipses to match the clusters best.

Figure 4 demonstrates this algorithm for the exemplary position Rx7D2 (see floorplan in Figure 1) for the first cluster. From Figure 4b, one can see dense SAGE estimates at $(\mathrm{AoA}/\mathrm{AoD}) = (40°/30°)$ with stronger power, the APS/SAGE plot (Figure 4a) shows a (wide) peak there, too. The extent of the cluster is now estimated by fitting an ellipse visually to the SAGE estimates. One has to take care that the cluster is not defined too large. The SAGE estimates around $(\mathrm{AoA}/\mathrm{AoD}) = (15°/30°)$ already belong to another cluster, as one can see from the SAGE plot. This method is repeated, until all clusters of an environment are identified, i.e. there are no more significant groups of MPCs to combine.

### *C. Cluster allocation*

Characteristics of the defined clusters were gathered by using the SAGE estimates allocated to clusters. The allocation was done for each scenario by the following algorithm.

1. SAGE estimation provides an indexed set of complex weights $\underline{\hat{A}}_k$, AoAs $\underline{\hat{\varphi}}_{\mathrm{Rx},k}$, and AoDs $\underline{\hat{\varphi}}_{\mathrm{Tx},k}$ of the propagation paths, for each considered channel realisation $k$. The set $\underline{\hat{A}}_k$ is indexed by
$$\underline{\hat{A}}_k = \left(\hat{A}_k^{(1)} \quad \hat{A}_k^{(2)} \quad \cdots \quad \hat{A}_k^{(N_{\mathrm{p},k})}\right), \tag{3}$$
where each of the sets contain $N_{\mathrm{p},k}$ (the number of resolved paths in the $k$th channel realisation) elements, at most 49 (corresponding to the model order). Equal indexing is done for $\underline{\hat{\varphi}}_{\mathrm{Rx},k}$, and $\underline{\hat{\varphi}}_{\mathrm{Tx},k}$.
Those sets are collected in $\hat{\mathbf{\Theta}}_k$ given by
$$\hat{\mathbf{\Theta}}_k = \left(\underline{\hat{A}}_k \quad \underline{\hat{\varphi}}_{\mathrm{Rx},k} \quad \underline{\hat{\varphi}}_{\mathrm{Tx},k}\right) = \mathrm{SAGE}(\mathbf{H}_k), \tag{4}$$
describing all resolved (estimated) paths for the $k$th channel realisation, where $\mathrm{SAGE}(\cdot)$ represents the estimates returned by the SAGE algorithm.

2. For each cluster $l$, we allocate the SAGE estimates enclosed by the defined ellipse and collect them in cluster sets $\mathcal{C}_l$ by

$$\mathcal{C}_l = \left(\tilde{\boldsymbol{\Theta}}_{1l} \;\; \tilde{\boldsymbol{\Theta}}_{2l} \;\; \cdots \;\; \tilde{\boldsymbol{\Theta}}_{Kl}\right), \quad l = 1 \ldots N_c, \qquad (5)$$

where $N_c$ denotes the number of clusters in the considered scenario and $\tilde{\boldsymbol{\Theta}}_{kl}$ is a subset of $\boldsymbol{\Theta}_k$ containing the corresponding SAGE estimates for the considered cluster $l$ and channel realisation $k$,

$$\tilde{\boldsymbol{\Theta}}_{kl} = \left(\underline{\tilde{A}}_{kl} \;\; \underline{\tilde{\varphi}}_{\mathrm{Rx},kl} \;\; \underline{\tilde{\varphi}}_{\mathrm{Tx},kl}\right), \quad \tilde{\boldsymbol{\Theta}}_{kl} \subset \hat{\boldsymbol{\Theta}}_k.$$

The indexed subsets $\underline{\tilde{A}}_{kl}$, $\underline{\tilde{\varphi}}_{\mathrm{Rx},kl}$, and $\underline{\tilde{\varphi}}_{\mathrm{Tx},kl}$ hold $N_{\mathrm{p},kl}$ (number of allocated paths in the $k$th realisation for the $l$th cluster) elements, each, and are again indexed as shown in (3). The sorting of the SAGE estimates into the cluster sets is done by geometrical considerations in the angular domain.

Figure 4c shows the double-directional APS of the exemplary measured scenario. Identified clusters are enclosed by ellipses; SAGE estimates falling within these ellipses are shown as white crosses. The other estimates are discarded.

### *D. Cluster directional spread estimation*

In this paper, we evaluate the root-mean-square (rms) *cluster* directional spread using SAGE estimates based on the specular wave model. This approach extends the view of a global directional spread of the environment. Here, we restrict the investigations to the azimuthal dispersion.

The directional spread of a propagation environment [4] using horizontal propagation is correctly defined by the second order moment of the *directions* at the Rx and Tx, where the direction is described by the azimuthal unity vector $\Omega$, hence[1]

$$\Omega^{\mathrm{rms}} = \sqrt{\frac{\int_{-\pi}^{\pi} \|e(\varphi) - \bar{\Omega}\|^2 |A(\varphi)|^2 \mathrm{d}\varphi}{\int_{-\pi}^{\pi} |A(\varphi)|^2 \mathrm{d}\varphi}} \qquad (6)$$

with

$$\bar{\Omega} = \left(\int_{-\pi}^{\pi} |A(\varphi)|^2 \mathrm{d}\varphi\right)^{-1} \int_{-\pi}^{\pi} e(\varphi) |A(\varphi)|^2 \mathrm{d}\varphi, \qquad (7)$$

where the integration over the whole unit sphere $\mathcal{S}$ is performed with $\Omega^{\mathrm{rms}}$ denoting the directional spread and $|A(\varphi)|^2$ the APS and $\|\cdot\|^2$ the vector norm.

Practically, multipath clusters in indoor scenarios show very low directional spreads. For small values of the directional spread we can approximate this value by the well-known angular spread [15] (in radians), which is given by

$$\varphi^{\mathrm{rms}} = \sqrt{\frac{\int_{-\pi}^{\pi} (\varphi - \bar{\varphi})^2 |A(\varphi)|^2 \mathrm{d}\varphi}{\int_{-\pi}^{\pi} |A(\varphi)|^2 \mathrm{d}\varphi}}, \text{ with } \bar{\varphi} = \frac{\int_{-\pi}^{\pi} \varphi |A(\varphi)|^2 \mathrm{d}\varphi}{\int_{-\pi}^{\pi} |A(\varphi)|^2 \mathrm{d}\varphi}, \qquad (8)$$

[1]In a cartesian coordinate system, $\Omega$ is a vector given by $\Omega = e(\varphi) \doteq [\cos(\varphi), \sin(\varphi)]^T$, where $\varphi$ denotes the azimuth.

where $\varphi^{\mathrm{rms}}$ denotes the azimuthal spread. In these formulas, integration over the whole azimuth domain is performed[2].

In the case of the *cluster* directional spread [16], only those components that contribute to the considered cluster have to be accounted. As our propagation paths are assumed to be discrete, the integrals reduce to sums and can easily be evaluated. For estimation of the cluster directional spreads, we calculated the AoA and AoD rms directional spread for each cluster $l$, by using the powers and angles of all resolved paths in the cluster. The mean AoA and AoD were separately calculated by

$$\bar{\varphi}_{\mathrm{AoA/AoD},l} = \frac{\sum_{k=1}^{K} \sum_{n=1}^{N_{p,kl}} \tilde{\varphi}^{(n)}_{\mathrm{Rx/Tx},kl} |\tilde{A}^{(n)}_{kl}|^2}{\sum_{k=1}^{K} \sum_{n=1}^{N_{p,kl}} |\tilde{A}^{(n)}_{kl}|^2}, \qquad (9)$$

subsequently, the rms directional spread was obtained by

$$\hat{\varphi}^{\mathrm{rms}}_{\mathrm{AoA/AoD},l} = \sqrt{\frac{\sum_{k=1}^{K} \sum_{n=1}^{N_{p,kl}} (\tilde{\varphi}^{(n)}_{\mathrm{Rx/Tx},kl} - \bar{\varphi}_{\mathrm{AoA/AoD},l})^2 |\tilde{A}^{(n)}_{kl}|^2}{\sum_{k=1}^{K} \sum_{n=1}^{N_{p,kl}} |\tilde{A}^{(n)}_{kl}|^2}}, \qquad (10)$$

for each cluster $l$ in the AoA (Rx) and AoD (Tx) domain.

## IV. Results

In Figure 5a the cluster directional spreads for the previously considered environment (Figure 4) are shown.

Note that the cluster directional spread also depends on the size of the ellipses defining the clusters. However, provided the cluster is defined following the rules described in Section III-B, the cluster directional spread does not change significantly with the size of the enclosing ellipse. In [17] we showed that the proposed cluster spread estimator is nearly unbiased with relative estimation errors of around $10\%$ in the range from $1^\circ$ to $8^\circ$ rms directional spread.

A histogram of cluster directional spreads obtained from all environments is shown in Figure 5b and 5c. We usually observe larger AoA than AoD cluster spreads, as the transmitter was placed in a corridor. One can see that the AoA cluster directional spread mainly varies between 2 and 7 degrees, whereas the AoD cluster spread varies between 2 and 9 degree.

## V. Conclusions

Multi-path clusters were characterised based on indoor measurements gathered in an office environment at 5.2 GHz. Clusters were evaluated for 72 scenarios with a subset of 150 realisations each. Identification of clusters was done visually using the double-directional Bartlett APS jointly with SAGE estimates. Ellipses were defined to fit the clusters best. As we are considering the AoA/AoD-domain, the number

[2]We want to note that this definition is sometimes used for the global directional spread, even when multiple large clusters are observed, which is not sensible.

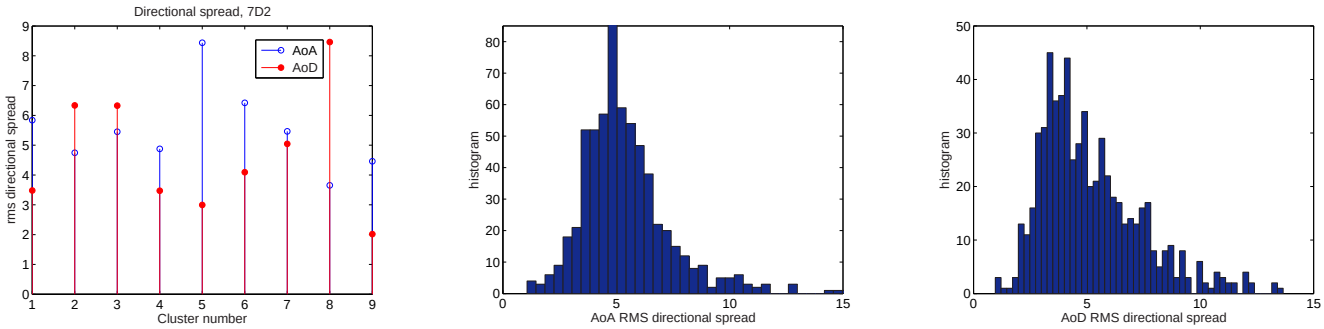


(a) (b) (c)

Fig. 5. (a) Directional cluster spread of exemplary environment, (b) Histogram of directional spreads seen from the receiver, (c) Histogram of directional spreads seen from transmitter

of identified clusters was usually larger than in comparable publications where only the AoA/delay-domain is considered.

We evaluated the rms cluster directional spreads for the AoAs and AoDs separately solely based on the SAGE estimates allocated to the clusters. As the transmitter was positioned in a corridor (providing a preferred propagation path), we observe different cluster azimuth spreads in the AoD domain than in the AoA domain. The cluster spreads are widely independent on the size of the cluster-defining enclosing ellipses. We found the AoA rms azimuth spread mainly between 2–7 degree, the AoD rms azimuth spread between 2–9 degree. Throughout literature, e.g. [2], [3], [5], [6], the directional spread was found to be much larger. The divergence with this paper results from the investigations done in the AoD domain instead of using the delay domain. Even a small, unresolvable deviation in the delay domain can result in completely different and well distinguishable AoDs. In the AoA/AoD-domain multipath clusters can be separated more precisely. For that reason, the cluster spreads have to be smaller in our evaluation.

## ACKNOWLEDGEMENTS

This work was partly sponsored by the European Network of Excellence NEWCOM. The PhD studies of two of the authors is co-financed by Elektrobit Testing Oy. We thank Markus Herdin (DoCoMo EuroLabs), Hüseyin Özcelik (INTHF) and Helmut Hofstetter (ftw.) for help with the measurements, T-Systems Nova GmbH for providing the receive antenna array, and Sven Semmelrodt of University of Kassel for providing the SAGE software package.

## REFERENCES

[1] K. Li, M. Ingram, and A. Van Nguyen, "Impact of clustering in statistical indoor propagation models on link capacity," *IEEE Transactions on Communications*, vol. 50, no. 4, pp. 521 – 523, April 2002.

[2] C.-C. Chong, C.-M. Tan, D. Laurenson, S. McLaughlin, M. Beach, and A. Nix, "A new statistical wideband spatio-temporal channel model for 5-GHz band WLAN systems," *IEEE Journal on Selected Areas in Communications*, vol. 21, no. 2, pp. 139 – 150, Feb. 2003.

[3] Q. H. Spencer, B. D. Jeffs, M. A. Jensen, and A. L. Swindlehurst, "Modeling the statistical time and angle of arrival characteristics of an indoor multipath channel," *IEEE Journal on Selected Areas in Communications*, vol. 18, pp. 347 – 359, March 2000.

[4] B. H. Fleury, "First- and second-order characterization of direction dispersion and space selectivity in the radio channel," *IEEE Transactions on Information Theory*, vol. IT-46, no. 6, pp. 2027–2044, September 2000.

[5] K. Yu, Q. Li, D. Cheung, and C. Prettie, "On the tap and cluster angular spreads of indoor WLAN channels," in *Proceedings of IEEE Vehicular Technology Conference Spring 2004*, Milano, Italy, May 17–19, 2004.

[6] A. S. Y. Poon and M. Ho, "Indoor multiple-antenna channel characterization from 2 to 8 GHz," *Proc. IEEE ICC*, vol. 5, pp. 3519–3523, May 2003.

[7] H. Özcelik, "Indoor MIMO channel models," Ph.D. dissertation, Institut für Nachrichtentechnik und Hochfrequenztechnik, Technische Universität Wien, Vienna, Austria, December 2004, downloadable from www.nt.tuwien.ac.at/mobile/theses_finished.

[8] R. Thomä, D. Hampicke, A. Richter, G. Sommerkorn, A. Schneider, U. Trautwein, and W. Wirnitzer, "Identification of time-variant directional mobile radio channels," *IEEE Transactions on Instrumentation and Measurement*, vol. 49, pp. 357–364, April 2000.

[9] P. Lehne, F. Aanvik, J. Bic, P. Pajusco, M. Grigat, I. Gaspard, and U. Martin, "Calibration of mobile radio channel sounders," *COST 259, TD(98)088*, Duisburg, September 23–25, 1998.

[10] B. H. Fleury, M. Tschudin, R. Heddergott, D. Dahlhaus, and K. I. Pedersen, "Channel parameter estimation in mobile radio environments using the SAGE algorithm," *IEEE Journal on Selected Areas in Communications*, no. 3, pp. 434–450, 17 1999.

[11] S. Semmelrodt, R. Kattenbach, and H. Früchting, "Toolbox for spectral analysis and linear prediction of stationary and non-stationary signals," *COST 273 TD(04)019*, Athens, Greece, January 26–28, 2004.

[12] M. Bengtsson and B. Volcker, "On the estimation of azimuth distributions and azimuth spectra," *IEEE Vehicular Technology Conference*, vol. 3, no. 54, pp. 1612 – 1615, October 07–11, 2001, Atlantic City, NJ, USA.

[13] M. Steinbauer, A. Molisch, and E. Bonek, "The double-directional radio channel," *IEEE Antennas and Propagation Magazine*, vol. 43, no. 4, pp. 51 – 63, Aug. 2001.

[14] M. Bartlett, "Smoothing periodograms from time series with continuous spectra," *Nature*, vol. No. 161, 1948.

[15] P. Eggers, "Angular propagation descriptions relevant for base station adaptive antenna operations," *Kluwer Wireless Personal Communications, Special Issue on SDMA*, vol. 11, pp. 3–29, 1999.

[16] A. Kuchar, M. Tangemann, and E. Bonek, "A real-time DOA-based smart antenna processor," *IEEE Transactions on Vehicular Technology*, vol. 51, no. 6, pp. 1279–1293, November 2002.

[17] N. Czink and X. Yin, "Estimation of cluster angular spread in MIMO indoor environments," 2005, submitted to SPWC'05, London, UK.